

Electron Beam Aberration Correction Using Optical Near Fields

Andrea Konečná¹ and F. Javier García de Abajo^{1,2,*}

¹*ICFO-Institut de Ciències Fotoniques, The Barcelona Institute of Science and Technology, 08860 Castelldefels (Barcelona), Spain*

²*ICREA-Institució Catalana de Recerca i Estudis Avançats, Passeig Lluís Companys 23, 08010 Barcelona, Spain*



(Received 24 April 2020; accepted 1 July 2020; published 17 July 2020)

The interaction between free electrons and optical near fields is attracting increasing attention as a way to manipulate the electron wave function in space, time, and energy. Relying on currently attainable experimental capabilities, we design optical near-field plates to imprint a lateral phase on the electron wave function that can largely correct spherical aberration without the involvement of electric or magnetic lenses in the electron optics, and further generate on-demand lateral focal spot profiles. Our work introduces a disruptive and powerful approach toward aberration correction based on light-electron interactions that could lead to compact and versatile time-resolved free-electron microscopy and spectroscopy.

DOI: [10.1103/PhysRevLett.125.030801](https://doi.org/10.1103/PhysRevLett.125.030801)

The development and widespread use of spatial light modulators have revolutionized optics by enabling an increasing degree of control over light beam propagation. Likewise, the extension of this concept to electron optics could provide the means for controlling the electron wave function and its interactions with atomic-scale samples. Electron microscopes already reach precise spatial and temporal control over the amplitude and phase of the wave function of beam electrons employed as sample probes. Over the last decades, costly and sophisticated arrangements of magnetostatic and electrostatic lenses have been engineered to eliminate electron-optics aberrations [1,2], making it possible to focus electron beams with sub-angstrom precision in state-of-the-art scanning transmission electron microscopes. These capabilities are crucial for atomic-scale imaging and spectroscopy [3,4].

Parallel efforts have led to the development of amplitude and phase reconstruction techniques such as ptychography [5] or electron tomography and holography [6], which have proved useful in both imaging low-contrast samples [7,8] and acquiring additional information on the sample, such as electric or magnetic field distributions [9–11]. An alternative approach has consisted in preparing electron beams with on-demand focal spot phase and intensity distributions designed to introduce phase contrast and selectively interact with targeted types of excitations such as plasmons of specific multipolar symmetry [12] or chiral modes and materials magnetic properties [13,14]. Such phase-shaped electron beams can be obtained through diffraction by a static phase plate [12,15–17] or ingenious use of lens aberrations [18,19]. A recent work also demonstrates programmable electron phase plates based on arrays of electrically biased transmission elements [20].

The interaction of free electrons with optical near fields in illuminated nanostructures opens exciting possibilities as a further mechanism to control the electron wave function.

This phenomenon has been exploited to develop the so-called photon-induced near-field electron microscopy [21], which has been the subject of intense experimental [21–40] and theoretical [41–48] efforts. By synchronizing the arrival of ultrashort electron and laser pulses near the sample, the former can undergo stimulated absorption or emission of up to hundreds of photons [39,40]. This technique has been predicted to imprint optical phase on the lateral electron wave function [45], which has been demonstrated to generate vortex electron beams via photon-to-electron angular momentum transfer [37]. The synergistic combination of spatial light modulators and ultrafast electron microscopy constitutes a powerful platform for the control of free-electron wave functions, including the possibility of compensating beam aberrations and shaping the focal spot. While other alternatives to traditional electron-optics components have been suggested, such as using nanofabricated structures or thin films for wave front shaping and correction [49,50], our target is to introduce a more versatile and tunable solution.

In this Letter, we theoretically demonstrate the correction of spherical aberration in an electron beam upon transmission through an illuminated thin film, where light-electron phase transfer compensates for the undesired deviation of the transverse electron wave function from a spherical wave front, thereby resulting in nearly unaberrated focusing down to subangstrom focal spots. The proposed implementation of this type of photonic aberration corrector (PAC) in an electron microscope is schematically depicted in Fig. 1, where the new element is placed after the condenser along the electron optical path in order to imprint the required phase on the electron wave function to compensate for the aberration produced by subsequent electron-optics focusing elements. The PAC consists of an optically opaque electron-transparent thin film (e.g., a metal film deposited on a Si₃N₄ membrane, as

already used in photon-induced near-field electron microscopy studies [25,35], but we discuss additional options in Sec. S3 of the Supplemental Material [51]) on which a lateral optical pattern is projected with diffraction-limited spatial resolution. Electron interaction with semi-infinite light fields [35] in this film then produces energy sidebands in the transmitted electrons that can be optimized to accommodate $\sim 1/3$ of the electrons in the first sideband (i.e., electrons that have gained one photon energy). A monochromator inserted right after the PAC removes the rest of the energy sidebands before entering an electron-optics module for focusing at the sample. Aberration correction is thus performed through the PAC phase plate, which represents an alternative to traditional aberration correctors. This type of design inherits the flexibility of light patterning through spatial light modulators, here demonstrated for aberration correction, but also enabling arbitrary shaping of the electron focal spot.

Electron beam propagation through the electron microscope.—We represent fast electrons by their space- and time-dependent wave function $\psi_z(\mathbf{R})e^{-i\mathcal{E}_0 t}$, where we consider monochromatic electrons of energy \mathcal{E}_0 that depend on transverse coordinates $\mathbf{R} = (x, y)$ at each propagation plane determined by z . Free propagation from z' to z is described by the expression [44,52]

$$\psi_z(\mathbf{R}) = \int \int \frac{d^2\mathbf{Q}d^2\mathbf{R}'}{(2\pi)^2} e^{i[\mathbf{Q}\cdot(\mathbf{R}-\mathbf{R}') + q_z(z-z')]} \psi_{z'}(\mathbf{R}'),$$

where the outer integral extends over transverse wave vectors \mathbf{Q} , $q_z = \sqrt{q_0^2 - Q^2}$ is the longitudinal wave vector, $\hbar\mathbf{q}_0 = m_e\mathbf{v}$ and \mathbf{v} are the average electron momentum and velocity vectors, respectively, $\gamma = 1/\sqrt{1 - v^2/c^2}$ is the Lorentz factor, m_e is the electron rest mass, and c is the speed of light in vacuum. In what follows, we focus on electron beams of well-defined chirality, characterized by an azimuthal orbital quantum number m , such that the wave function takes the form $\psi_z(\mathbf{R}) = \psi_z(R)e^{im\varphi}$, where (R, φ) are polar coordinates. Additionally, electrons in microscopes are collimated and therefore safely described in the paraxial approximation, for which $q_z \approx q_0 - Q^2/2q_0$. These considerations allow us to carry out some of the above integrals to find [51]

$$\begin{aligned} \psi_z(R) &= (\mathcal{F}_{z-z'}^m \cdot \psi_{z'})|_R \\ &\equiv (-i)^{m+1} \xi_{z-z'} e^{iq_0(z-z')} \\ &\quad \times \int_0^\infty R' dR' J_m(\xi_{z-z'} R R') e^{i\xi_{z-z'}(R^2+R'^2)/2} \psi_{z'}(R'), \end{aligned} \quad (1)$$

where $\xi_{z-z'} = q_0/(z - z')$, J_m is a Bessel function, and we implicitly define the free-propagation operator \mathcal{F}^m using matrix notation with a dot standing for integration over the radial coordinate R .

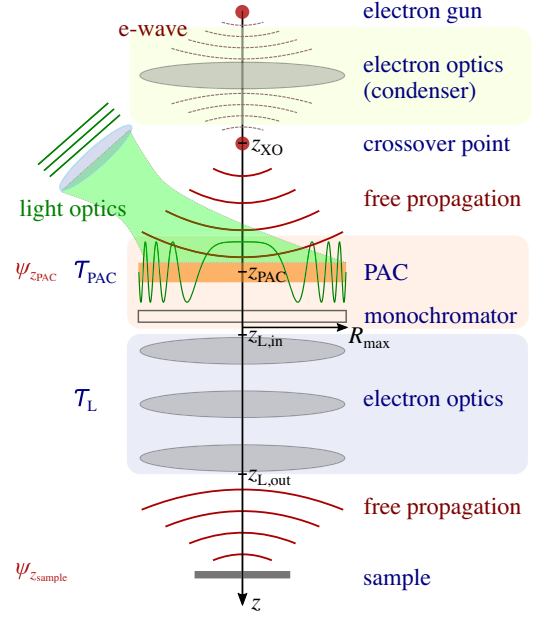


FIG. 1. Proposed experimental arrangement incorporating a photonic aberration corrector (PAC) to mitigate electron spherical aberration through an electron optical phase plate. The PAC module (light orange frame) is placed just before the electron-optics focusing module (electromagnetic lenses inside the light blue frame) at a distance $z_{L,in} - z_{XO}$ from the crossover point. A coherent electron wave is prepared by condenser lenses placed after an electron gun. Both the transmitted beam and the light wave prepared by a spatial light modulator are restricted by a circular aperture of radius R_{\max} .

Transmission through the microscope sketched in Fig. 1 results in an electron wave function at the sample given by

$$\psi_{z_{\text{sample}}} = \mathcal{F}_{z_{\text{sample}}-z_{L,\text{out}}}^m \cdot \mathcal{T}_L \cdot \mathcal{F}_{z_{L,\text{in}}-z_{\text{PAC}}}^m \cdot \mathcal{T}_{\text{PAC}} \cdot \psi_{z_{\text{PAC}}}, \quad (2)$$

where $\psi_{z_{\text{PAC}}}$ represents the electron incident on the plane of the corrector at z_{PAC} , while \mathcal{T}_{PAC} and \mathcal{T}_L account for transmission through the PAC and electron lenses (orange and blue frames in Fig. 1, respectively). For a thin lens, the latter is well described by [53,54]

$$\mathcal{T}_L|_{RR'} = \delta(R - R') e^{i\chi(\theta)} e^{-iq_0 R^2/2f} \Theta(R_{\max} - R), \quad (3)$$

where f is the focal distance, a pupil blocks propagation above a radial distance R_{\max} , and the phase $\chi(\theta)$ accounts for aberrations in the lenses as a function of exit angle $\theta = R/(z_{\text{sample}} - z_{L,\text{out}})$. Here, we concentrate on spherical aberration, so we express $\chi(\theta) = C_3 q_0 \theta^4/4$ in terms of the (length) coefficient C_3 [52,55]. For simplicity, in what follows we consider a spherical wave $\psi_{z_{\text{PAC}}}(R) \propto e^{iq_0 R^2/2(z_{\text{PAC}}-z_{XO})}$ with $m = 0$ emerging from a perfect point-like crossover that can be produced by another set of condenser lenses placed after the electron source and

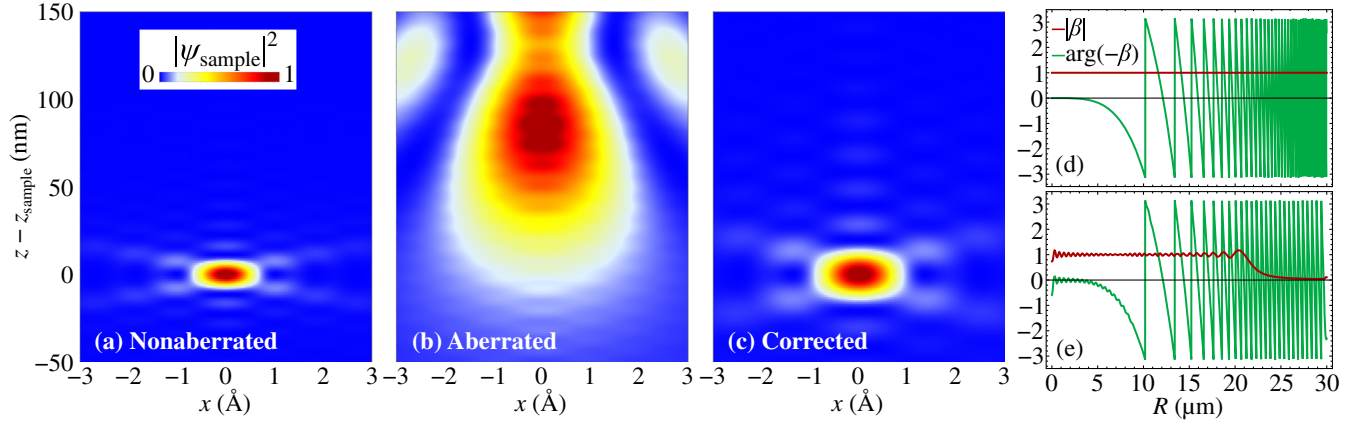


FIG. 2. Spatial dependence of the electron intensity focus at the sample. We plot the normalized beam electron density $|\psi_{\text{sample}}|^2$ [Eq. (2)] obtained through (a) aberration-free electron optics; (b) electron optics introducing spherical aberration with $C_3 = 1$ mm; and (c) same as (b) including a PAC module. We consider 60-keV electrons, a focal distance $f = 1$ mm, $z_L - z_{\text{xo}} = 40f$, and an aperture $R_{\text{max}} = 30$ μm . The corrected beam profile in (c) is calculated by using a realistic spatial dependence of the coupling parameter β as a function of radial distance R in the PAC [panel (e), obtained from Eqs. (6) and (8) with $\lambda_0 = 500$ nm light wavelength], which differs from the ideal β that is needed to perfectly correct the aberration [panel (d), Eq. (7)].

preceding the PAC. In practice, the condenser lenses together with collimating apertures provide lateral coherence of the electron beam over the aperture restricted by R_{max} , as needed for a correct performance of the PAC. We note that the PAC can also correct for aberrations introduced by the preceding lenses, but for demonstration purposes, here we only consider the electron-optics aberration produced by the objective lens placed after the PAC. Additionally, we take the PAC to coincide with the near and far sides of the optical lenses at the virtual plane $z = z_L$.

In the absence of aberrations ($\chi = 0$), $\psi_{z_{\text{sample}}}$ is focused at a position $z = z_{\text{sample}}$ determined by the lens formula $1/(z_{\text{sample}} - z_L) + 1/(z_L - z_{\text{xo}}) = 1/f$ [51]. This is illustrated in Fig. 2(a) for 60-keV electrons (~ 5 pm wavelength) with $z_L - z_{\text{xo}} = 40f$ (implying $z_{\text{xo}} - z_L \approx f$), $f = 1$ mm, and $R_{\text{max}} = 30$ μm . The focal spot is limited by diffraction at the aperture, yielding a $\psi_{z_{\text{sample}}} \sim J_1(R/\Delta)$ transverse profile of subangstrom width $\sim \Delta = f/q_0 R_{\text{max}} = 0.26$ Å. In contrast, a typical spherical aberration corresponding to $C_3 = 1$ mm produces a substantially broadened and shifted focus [Fig. 2(b)], accompanied by satellite foci along the optical axis.

Electron optical phase plate.—We intend to cancel the aberration phase χ by imprinting an additional phase on the electron wave function through the interaction with an optical near field [35,44,45]. For this purpose, we consider an optically opaque electron-transparent film subject to external illumination, a configuration that has been demonstrated to produce large coupling to the electrons [35]. We assume that inelastic scattering due to interaction with the film material can be neglected, while the additional phase acquired through this interaction should only contribute as a position-independent overall factor. The condition of weak inelastic scattering is met by thin metal films

with thickness < 10 nm, well below the electron inelastic mean free path [51,56]. Alternatively, a thin dielectric membrane can be used together with more intense optical illumination, as we demonstrate in Sec. S3 of the Supplemental Material [51].

The transmitted electron wave function consists of sidebands of energies $\mathcal{E}_0 + \hbar\ell\omega_0$ separated from the incident energy by multiples ℓ (< 0 for loss, > 0 for gain) of the photon energy $\hbar\omega_0$. In the nonrecoil approximation, the wave function associated with each transmitted sideband ℓ consists of the incident wave function times a multiplicative factor accounted for by the operator [35,46]

$$\mathcal{T}_{\text{PAC}}|_{RR'} = \delta(R - R')J_\ell(2|\beta|)e^{i\ell \arg\{-\beta\}}, \quad (4)$$

where the coupling coefficient

$$\beta(\mathbf{R}) = \frac{e}{\hbar\omega_0} \int_{-\infty}^{\infty} dz E_z(\mathbf{R}, z) e^{-i\omega_0 z/v} \quad (5)$$

captures the electron-light interaction through the (along-the-beam) E_z component of the optical electric-field amplitude, which bears a dependence on transverse coordinates \mathbf{R} that can be controlled through a spatial light modulator. We first consider axially symmetric illumination [implying $m = 0$ in Eq. (2)] and express the incident optical field $E_z = \int_0^{k_0} dk_{\parallel} J_0(k_{\parallel} R) e^{ik_z z} \alpha_{k_{\parallel}}$ as a combination of cylindrical Bessel waves with in- and out-of-plane wave vector components k_{\parallel} and $k_z = \sqrt{k_0^2 - k_{\parallel}^2}$, respectively, limited by the free-space light wave vector $k_0 = \omega_0/c$. Upon insertion of this field into Eq. (5), we find

$$\beta(R) = \int_0^{k_0} k_{\parallel} dk_{\parallel} J_0(k_{\parallel} R) \beta_{k_{\parallel}}, \quad (6)$$

where the coefficient $\beta_{k_{\parallel}}$ is proportional to $\alpha_{k_{\parallel}}$ and also includes light components reflected at the film [35]; we stress that $\beta_{k_{\parallel}}$ can therefore be controlled through the applied angular light profile $\alpha_{k_{\parallel}}$.

Design of the PAC field profile.—We now design the PAC based on an electron optical phase plate in which $\ell = 1$ is selected, while other sidebands ($\ell \neq 1$) are filtered out by a monochromator (Fig. 1), using for example a Wien filter [1] (easily capable of separating peaks with an energy difference $\hbar\omega_0 \sim 1$ eV). The aberration phase χ introduced through \mathcal{T}_L [Eq. (3)] can then be eliminated from Eq. (2) by setting

$$\arg\{-\beta(R)\} = -\chi(\theta) \quad (7)$$

in \mathcal{T}_{PAC} [Eq. (4)], where $R = \theta(z_{\text{sample}} - z_L)$. We can maximize the current by imposing $|\beta| = \beta_0 \approx 0.92$, which yields an absolute maximum fraction of the $\ell = 1$ sideband $J_1^2(2\beta_0) \approx 34\%$ [51]. The PAC then involves a reduction in electron current by a factor of $\sim 2/3$, which, together with beam losses due to interaction with the PAC material, represents a drawback compared to traditional solutions for aberration correction in which most of the beam current is transmitted. The spatial dependence of $\beta = -\beta_0 e^{-i\chi}$ required to produce perfect aberration correction and maximum $\ell = 1$ current is presented in Fig. 2(d) according to Eq. (7) for $\mathcal{E}_0 = 60$ keV and $f = C_3 = 1$ mm. However, optical diffraction at the used finite light wavelength $\lambda_0 = 2\pi/k_0$ limits the profile of β that can be achieved in practice using far-field illumination. We find a nearly optimum realistic profile by setting $\beta = -\beta_0 e^{-i\chi}$ in Eq. (6) and approximately inverting this equation to yield

$$\beta_{k_{\parallel}} = -\beta_0 \int_0^{R_{\text{max}}} R dR J_0(k_{\parallel} R) e^{-i\chi[R/(z_{\text{sample}} - z_L)]} \quad (8)$$

(this inversion is only exact in the $k_0 R_{\text{max}} \gg 1$ limit). The coupling coefficient obtained by inserting Eq. (8) back into Eq. (6) is plotted in Fig. 2(e) for a photon wavelength $\lambda_0 = 500$ nm, which resembles the perfect-correction coefficient of Fig. 2(d) up to $R \sim 20 \mu\text{m}$, but deviates substantially from that target value at larger R (i.e., where the phase χ exhibits rapid variations over a distance $\sim \lambda_0$). Although the resulting corrected beam profile plotted in Fig. 2(c) is not perfect, it still provides an impressive improvement in electron focusing compared to the aberrated spot shown in Fig. 2(b) [51]. We note that the degree of correction increases when λ_0 is made smaller relative to R_{max} , as we show in Fig. 3, which further predicts a remarkable aberration compensation using blue light. We also verified that aberration correction by the PAC does not

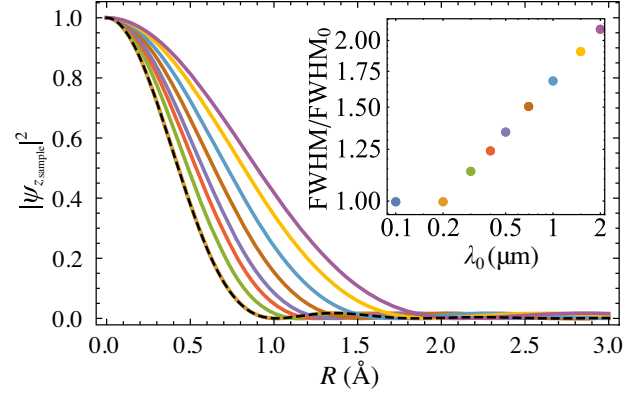


FIG. 3. Approaching perfect aberration correction. We show the focal spot profile obtained with the same parameters as in Fig. 2(c) using light of different wavelength λ_0 . The inset shows the spot FWHM normalized to the unaberrated one (FWHM_0 , corresponding to the dashed black curve in the main plot) and provides a color legend for the main plot.

introduce any undesired beam tails (see Fig. S5 in the Supplemental Material [51]).

The PAC can be fed using light with definite chirality m [i.e., $E_z(\mathbf{R}, z) = E_z(R, z)e^{im\varphi_R}$, which directly translates through Eqs. (4) and (5) into $\mathcal{T}_{\text{PAC}} \propto e^{im\varphi_R}$], still described by Eqs. (6) and (8) with J_0 substituted by J_m . Results for the transverse profile of the electron focus using chiral PACs with $m = 1$ and 3 are compared with the $m = 0$ profile in Fig. 4, revealing the formation of donuts

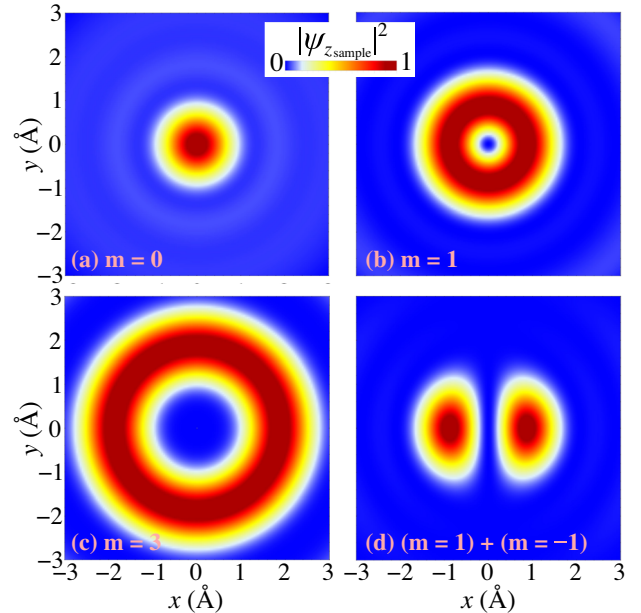


FIG. 4. Manipulation of the focal spot profile. Transverse cuts of electron focal spots obtained by correcting spherical aberration under the same conditions as in Fig. 2(c) but using light fields with the indicated symmetry: $e^{im\varphi}$ azimuthal dependence in (a)–(c) and $\cos\varphi$ in (d).

associated with an electron wave function of e^{imp} azimuthal symmetry. More complex profiles are possible, which should be reachable using a spatial light modulator to project light on the PAC. For example, Fig. 4(d) shows the result obtained by projecting a symmetric combination of $m = 1$ and $m = -1$ light.

Conclusion.—In summary, we propose the use of electron optical phase plates as a way of tailoring the amplitude and phase of the electron-transverse wave function in an electron beam. Specifically, we theoretically demonstrate correction of spherical aberration without the involvement of complex electron-optics elements. This concept can be straightforwardly applied to eliminate any undesired distortions introduced by electron optics in both standard and ultrafast electron microscopes. Although we apply analytical methods to produce a proof-of-principle design, improvement in the capabilities of such phase plates could be gained through machine learning, which should enable the design of more complex electron spot shapes or correction of a general combination of aberrations following the example of light optics [57]. Ultimately, iterative improvement of the PAC could be attained through a feedback loop involving measurement of the electron spot and modification of the projected light profile. Additionally, temporal manipulation of the imprinted optical phase offers interesting possibilities for the exploration of sample dynamics through time-varying electron spot profiles. The versatility and compactness of electron optical phase plates hold potential for active control of electron wave functions beyond the present application in aberration correction.

We thank Mathieu Kociak, Albert Polman, and Claus Ropers for helpful and enjoyable discussions. This work has been supported in part by ERC (Advanced Grant 789104-eNANO), the Spanish MINECO (MAT2017-88492-R and SEV2015-0522), the Catalan CERCA Program, and Fundació Privada Cellex.

*Corresponding author.

javier.garciadeabajo@nanophotonics.es

- [1] P. Hawkes and J. Spence, *Springer Handbook of Microscopy* (Springer Nature, Switzerland, AG, 2019).
- [2] M. Haider, H. Rose, S. Uhlemann, E. Schwan, B. Kabius, and K. Urban, *Ultramicroscopy* **75**, 53 (1998).
- [3] P. E. Batson, N. Dellby, and O. L. Krivanek, *Nature (London)* **418**, 617 (2002).
- [4] D. A. Muller, L. Fitting Kourkoutis, M. Murfitt, J. H. Song, H. Y. Hwang, J. Silcox, N. Dellby, and O. L. Krivanek, *Science* **319**, 1073 (2008).
- [5] Y. Jiang, Z. Chen, Y. Han, P. Deb, H. Gao, S. Xie, P. Purohit, M. W. Tate, J. Park, S. M. Gruner *et al.*, *Nature (London)* **559**, 343 (2018).
- [6] P. A. Midgley and R. E. Dunin-Borkowski, *Nat. Mater.* **8**, 271 (2009).
- [7] H.-W. Fink, H. Schmid, E. Ermantraut, and T. Schulz, *J. Opt. Soc. Am. A* **14**, 2168 (1997).
- [8] F. S. Yasin, T. R. Harvey, J. J. Chess, J. S. Pierce, C. Ophus, P. Ercius, and B. J. McMorran, *Nano Lett.* **18**, 7118 (2018).
- [9] M. R. McCartney, N. Agarwal, S. Chung, D. A. Cullen, M.-G. Han, K. He, L. Li, H. Wang, L. Zhou, and D. J. Smith, *Ultramicroscopy* **110**, 375 (2010).
- [10] O. Nicoletti, F. de la Peña, R. K. Leary, D. J. Holland, C. Ducati, and P. A. Midgley, *Nature (London)* **502**, 80 (2013).
- [11] K. Shibata, A. Kovács, N. S. Kiselev, N. Kanazawa, R. E. Dunin-Borkowski, and Y. Tokura, *Phys. Rev. Lett.* **118**, 087202 (2017).
- [12] G. Guzzinati, A. Beche, H. Lourenco-Martins, J. Martin, M. Kociak, and J. Verbeeck, *Nat. Commun.* **8**, 14999 (2017).
- [13] S. M. Lloyd, M. Babiker, G. Thirunavukkarasu, and J. Yuan, *Rev. Mod. Phys.* **89**, 035004 (2017).
- [14] J. Rusz and S. Bhowmick, *Phys. Rev. Lett.* **111**, 105504 (2013).
- [15] J. Verbeeck, H. Tian, and P. Schattschneider, *Nature (London)* **467**, 301 (2010).
- [16] B. J. McMorran, A. Agrawal, I. M. Anderson, A. A. Herzing, H. J. Lezec, J. J. McClelland, and J. Unguris, *Science* **331**, 192 (2011).
- [17] R. Shiloh, Y. Lereah, Y. Lilach, and A. Arie, *Ultramicroscopy* **144**, 26 (2014).
- [18] P. Schattschneider, M. Stöger-Pollach, and J. Verbeeck, *Phys. Rev. Lett.* **109**, 084801 (2012).
- [19] L. Clark, A. Béch  , G. Guzzinati, A. Lubk, M. Mazilu, R. Van Boxem, and J. Verbeeck, *Phys. Rev. Lett.* **111**, 064801 (2013).
- [20] J. Verbeeck, A. B    , K. M  ller-Caspary, G. Guzzinati, M. A. Luong, and M. Den Hertog, *Ultramicroscopy* **190**, 58 (2018).
- [21] B. Barwick, D. J. Flannigan, and A. H. Zewail, *Nature (London)* **462**, 902 (2009).
- [22] F. O. Kirchner, A. Gliserin, F. Krausz, and P. Baum, *Nat. Photonics* **8**, 52 (2014).
- [23] L. Piazza, T. T. A. Lummen, E. Qui      , Y. Murooka, B. Reed, B. Barwick, and F. Carbone, *Nat. Commun.* **6**, 6407 (2015).
- [24] A. Feist, K. E. Echternkamp, J. Schauss, S. V. Yalunin, S. Sch  fer, and C. Ropers, *Nature (London)* **521**, 200 (2015).
- [25] T. T. A. Lummen, R. J. Lamb, G. Berruto, T. LaGrange, L. D. Negro, F. J. Garc     de Abajo, D. McGrouther, B. Barwick, and F. Carbone, *Nat. Commun.* **7**, 13156 (2016).
- [26] K. E. Echternkamp, A. Feist, S. Sch  fer, and C. Ropers, *Nat. Phys.* **12**, 1000 (2016).
- [27] C. Kealhofer, W. Schneider, D. Ehberger, A. Ryabov, F. Krausz, and P. Baum, *Science* **352**, 429 (2016).
- [28] A. Ryabov and P. Baum, *Science* **353**, 374 (2016).
- [29] G. M. Vanacore, A. W. P. Fitzpatrick, and A. H. Zewail, *Nano Today* **11**, 228 (2016).
- [30] Y. Morimoto and P. Baum, *Nat. Phys.* **14**, 252 (2018).
- [31] M. Koz    , J. McNeur, K. J. Leedle, H. Deng, N. Sch          , A. Ruehl, I. Hartl, J. S. Harris, R. L. Byer, and P. Hommelhoff, *Nat. Commun.* **8**, 14342 (2017).
- [32] A. Feist, N. Bach, T. D. N. Rubiano da Silva, M. M      , K. E. Priebe, T. Domr    , J. G. Gatzmann, S. Rost, J. Schauss, S. Strauch *et al.*, *Ultramicroscopy* **176**, 63 (2017).

- [33] K. E. Priebe, C. Rathje, S. V. Yalunin, T. Hohage, A. Feist, S. Schäfer, and C. Ropers, *Nat. Photonics* **11**, 793 (2017).
- [34] E. Pomarico, I. Madan, G. Berruto, G. M. Vanacore, K. Wang, I. Kaminer, F. J. García de Abajo, and F. Carbone, *ACS Photonics* **5**, 759 (2018).
- [35] G. M. Vanacore, I. Madan, G. Berruto, K. Wang, E. Pomarico, R. J. Lamb, D. McGrouther, I. Kaminer, B. Barwick, F. J. García de Abajo, and F. Carbone, *Nat. Commun.* **9**, 2694 (2018).
- [36] Y. Morimoto and P. Baum, *Phys. Rev. A* **97**, 033815 (2018).
- [37] G. M. Vanacore, G. Berruto, I. Madan, E. Pomarico, P. Biagioni, R. J. Lamb, D. McGrouther, O. Reinhardt, I. Kaminer, B. Barwick *et al.*, *Nat. Mater.* **18**, 573 (2019).
- [38] K. Wang, R. Dahan, M. Shentcis, Y. Kauffmann, S. Tsesses, and I. Kaminer, *Nature (London)* **582**, 50 (2020).
- [39] S. Nehemia, R. Dahan, M. Shentcis, O. Reinhardt, Y. Adiv, K. Wang, O. Beer, Y. Kurman, X. Shi, M. H. Lynch, and I. Kaminer, [arXiv:1909.00757](https://arxiv.org/abs/1909.00757).
- [40] O. Kfir, H. Lourenço-Martins, G. Storeck, M. Sivils, T. R. Harvey, T. J. Kippenberg, A. Feist, and C. Ropers, *Nature (London)* **582**, 46 (2020).
- [41] F. J. García de Abajo, A. Asenjo Garcia, and M. Kociak, *Nano Lett.* **10**, 1859 (2010).
- [42] S. T. Park, M. Lin, and A. H. Zewail, *New J. Phys.* **12**, 123028 (2010).
- [43] S. T. Park and A. H. Zewail, *J. Phys. Chem. A* **116**, 11128 (2012).
- [44] F. J. García de Abajo, B. Barwick, and F. Carbone, *Phys. Rev. B* **94**, 041404(R) (2016).
- [45] W. Cai, O. Reinhardt, I. Kaminer, and F. J. García de Abajo, *Phys. Rev. B* **98**, 045424 (2018).
- [46] V. Di Giulio, M. Kociak, and F. J. García de Abajo, *Optica* **6**, 1524 (2019).
- [47] O. Kfir, *Phys. Rev. Lett.* **123**, 103602 (2019).
- [48] O. Reinhardt, C. Mechel, M. Lynch, and I. Kaminer, [arXiv:1907.10281](https://arxiv.org/abs/1907.10281).
- [49] V. Grillo, A. H. Tavabi, E. Yucelen, P.-H. Lu, F. Venturi, H. Larocque, L. Jin, A. Savenko, G. C. Gazzadi, R. Balboni *et al.*, *Opt. Express* **25**, 21851 (2017).
- [50] R. Shiloh, R. Remez, P.-H. Lu, L. Jin, Y. Lereah, A. H. Tavabi, R. E. Dunin-Borkowski, and A. Arie, *Ultramicroscopy* **189**, 46 (2018).
- [51] See Supplemental Material at <http://link.aps.org/supplemental/10.1103/PhysRevLett.125.030801> for a derivation of Eq. (1), a calculation of the coupling coefficient β for thin films, additional elements of the simulation with the PAC and the electron lenses at the same virtual plane, further details on the PAC, and a comparison of electron spot profiles with and without aberration correction.
- [52] L. J. Allen, M. P. Oxley, and D. Paganin, *Phys. Rev. Lett.* **87**, 123902 (2001).
- [53] P. Hawkes, B. Lencová, and M. Lenc, *J. Microsc.* **179**, 145 (1995).
- [54] R. F. Egerton, *Physical Principles of Electron Microscopy: An Introduction to TEM, SEM, and AEM* (Springer, New York, 2005).
- [55] D. M. Paganin, T. C. Petersen, and M. A. Beltran, *Phys. Rev. A* **97**, 023835 (2018).
- [56] H. Shinotsuka, S. Tanuma, C. J. Powell, and D. R. Penn, *Surf. Interface Anal.* **47**, 871 (2015).
- [57] O. Albert, L. Sherman, G. Mourou, T. B. Norris, and G. Vdovin, *Opt. Lett.* **25**, 52 (2000).